Analysis of Droop Controlled Parallel Inverters in Islanded Microgrids

Mariani, Valerio; Vasca, Francesco; Guerrero, Josep M.

Analysis of Droop Controlled Parallel Inverters in Islanded Microgrids

V. Mariani [#1], F. Vasca [#2], J. M. Guerrero [*1]

Department of Engineering, University of Sannio
Piazza Roma 21, 82100 Benevento, Italy
[1] valerio.mariani@unisannio.it
[2] francesco.vasca@unisannio.it

* Department of Energy Technology, Aalborg University
Pontoppidanstræde 101, 9100 Aalborg, Denmark
[1] joz@et.aau.dk

Abstract—**Three-phase droop controlled inverters are widely used in islanded microgrids to interface distributed energy resources and to provide for the loads active and reactive powers demand. The assessment of microgrids stability, affected by the control and line parameters, is a stringent issue. This paper shows a systematic approach to derive a closed loop model of the microgrid and then to perform an eigenvalues analysis that highlights how the system's parameters affect the stability of the network. It is also shown that by means of a singular perturbation approach the resulting reduced order system well approximate the original full order system.**

Index Terms—**Power Systems, Islanded Microgrids, Small-Signal Stability Analysis, Singularly Perturbed Systems.**

Fig. 1. AC microgrid in islanded-mode with two inverters and two local loads.

I. INTRODUCTION

Microgrids consist of an interconnection of distributed energy resources, storages and loads arranged via various topologies. Tipically, each of the aforementioned elements uses inverters to interface to the network in order to ensure the proper behavior of the microgrid in the widest range of the working conditions. A widely used control technique for the distributed energy resources inverters is the droop control because it allows to properly support for the active and reactive power loads demand [1], [2], [3]. Because of the nonlinearity of the control technique, even in presence of microgrids with few inverters, the closed loop model of such systems may become very complex. Nevertheless, a precise and rigorous assessment of the stability of the microgrids is very important. Many papers show, through a small-signal approach and experimental validations, that the frequency droop control parameter, which is tipically designed in order to ensure the proper load sharing, strongly affects the stability of the system [4], [5], [6], [7]. More theoretical analysis of the influence of the control parameters on the stability of distributed generation systems with droop controlled inverters can be found in [8], [9], [10]. In this paper, a systematic approach to the modeling of three-phase AC microgrids with inverters under voltage and frequency droop controls is presented. In Sec. II a model of a three-phase AC microgrid consisting of two inverters connected via a resistive-inductive line and of two local resistive-inductive loads is obtained. Then, in Sec. III the closed-loop model and a corresponding reduced
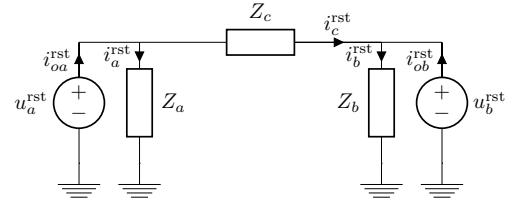
order model determined via a singular perturbation approach are presented. Numerical analysis of the full order model showing the time evolutions of the currents, the powers, the angle delay between the two inverters, the inverter frequencies is presented in Sec. IV. The models eigenlocus for increasing frequency control parameter and power filters time constants are investigated. By comparison, it is highlighted that the reduced order model is able to predict the instability for the same value of the frequency control parameter for which the full order model is unstable. Sec. V concludes the paper.

II. THREE-PHASE SYSTEM MODELING

An equivalent circuit of the three-phase AC microgrid under investigation is depicted in Fig. 1. Two inverters are connected by means of a balanced resistive-inductive line with phase impedances $Z_c = R_c + \jmath\omega L_c$. The two inverters have corresponding balanced resistive-inductive local loads with phase impedances $Z_a = R_a + \jmath\omega L_a$ and $Z_b = R_b + \jmath\omega L_b$, respectively. We assume that the k-th inverter, represented with the corresponding local load by the circuit depicted Fig. 2, provides the three-phase voltage sequence $u_k^{\mathrm{rst}} = \begin{bmatrix} u_k^r & u_k^s & u_k^t \end{bmatrix}^\top$ given by

$$\begin{bmatrix} u_k^r \\ u_k^s \\ u_k^t \end{bmatrix} = \sqrt{2} \begin{bmatrix} U_k \cos\theta_k \\ U_k \cos(\theta_k + 2/3\pi) \\ U_k \cos(\theta_k - 2/3\pi) \end{bmatrix}, \qquad (1)$$

with $k = a, b$ and where U_k, θ_k are the time-varying voltage amplitude and the time-varying angle of the k-th inverter

determined with respect the k-th local reference frame. Since we do not assume communication between the two inverters, the corresponding controls are not assumed to be synchronized in phase, i.e. $\theta_a(0)$ and $\theta_b(0)$ are independent. The three-phase k-th inverter output current sequence $i_{ok}^{\mathrm{rst}} = \begin{bmatrix} i_{ok}^r & i_{ok}^s & i_{ok}^t \end{bmatrix}^\top$ and local load current sequence $i_k^{\mathrm{rst}} = \begin{bmatrix} i_k^r & i_k^s & i_k^t \end{bmatrix}^\top$ are defined as

$$\begin{bmatrix} i_{ok}^r \\ i_{ok}^s \\ i_{ok}^t \end{bmatrix} = \sqrt{2} \begin{bmatrix} I_{ok}\cos(\theta_k + \varphi_k) \\ I_{ok}\cos(\theta_k + \varphi_k + 2/3\pi) \\ I_{ok}\cos(\theta_k + \varphi_k - 2/3\pi) \end{bmatrix}, \qquad (2)$$

and

$$\begin{bmatrix} i_k^r \\ i_k^s \\ i_k^t \end{bmatrix} = \sqrt{2} \begin{bmatrix} I_k\cos(\theta_k + \phi_k) \\ I_k\cos(\theta_k + \phi_k + 2/3\pi) \\ I_k\cos(\theta_k + \phi_k - 2/3\pi) \end{bmatrix}, \qquad (3)$$

with $k = a, b$ and where I_{ok}, I_k, φ_k and ϕ_k are the time-varying output current amplitude, the time-varying load current amplitude, the time-varying angle delay of the k-th output inverter current and the time-varying angle delay of the k-th load current with respect to the corresponding voltages instantaneous phases θ_k. Furthermore, the three-phase line current $i_c^{\mathrm{rst}} = \begin{bmatrix} i_c^r & i_c^s & i_c^t \end{bmatrix}^\top$ can be written as

$$\begin{bmatrix} i_c^r \\ i_c^s \\ i_c^t \end{bmatrix} = \sqrt{2} \begin{bmatrix} I_c\cos\theta_c \\ I_c\cos(\theta_c + 2/3\pi) \\ I_c\cos(\theta_c - 2/3\pi) \end{bmatrix}$$
$$= \sqrt{2} \begin{bmatrix} I_c\cos(\theta_a + x_a) \\ I_c\cos(\theta_a + x_a + 2/3\pi) \\ I_c\cos(\theta_a + x_a - 2/3\pi) \end{bmatrix}, \qquad (4a)$$

where θ_c is the time-varying angle determined with respect to the local line reference frame and $x_a = \theta_c - \theta_a$ is the angle delay between the angle of u_a and the angle of the line current i_c. Each k-th three-phase voltage and current is represented in a local $\alpha\beta$ reference frame by means of the well known Clarke transformation [11]

$$T = \frac{2}{3} \begin{bmatrix} 1 & -1/2 & -1/2 \\ 0 & \sqrt{3}/2 & -\sqrt{3}/2 \\ 1/2 & 1/2 & 1/2 \end{bmatrix} = \frac{2}{3} \begin{bmatrix} & T_{3\mathrm{to}2} \\ 1/2 & 1/2 & 1/2 \end{bmatrix}, \qquad (5)$$

with $T_{3\mathrm{to}2} \in \mathbb{R}^{2\times 3}$ being the matrix drawn from $T \in \mathbb{R}^{3\times 3}$ taking the first and the second row. For balanced three-wire systems the third row can be neglected. The inverse Clarke transformation is defined as

$$T^{-1} = \frac{3}{2} \begin{bmatrix} 2/3 & 0 & 2/3 \\ -1/3 & \sqrt{3}/3 & 2/3 \\ -1/3 & -\sqrt{3}/3 & 2/3 \end{bmatrix} = \frac{3}{2} \begin{bmatrix} & 2/3 \\ T_{2\mathrm{to}3} & 2/3 \\ & 2/3 \end{bmatrix}, \qquad (6)$$

with $T_{2\mathrm{to}3} \in \mathbb{R}^{3\times 2}$ being the matrix drawn from $T^{-1} \in \mathbb{R}^{3\times 3}$ taking the first and the second column. By applying the Kirchhoff voltage laws one obtains

$$L_k \frac{d}{dt} i_k^{\mathrm{rst}} = -R_k i_k^{\mathrm{rst}} + u_k^{\mathrm{rst}}, \qquad (7a)$$

$$L_c \frac{d}{dt} i_c^{\mathrm{rst}} = -R_c i_c^{\mathrm{rst}} + u_a^{\mathrm{rst}} - u_b^{\mathrm{rst}}, \qquad (7b)$$

where $k = a, b$. By representing (7) in the corresponding k-th $\alpha\beta$ local reference frame, that is by substituing to each voltage and current in (7) the corresponding representation in terms of $\alpha\beta$ components given by

$$y_j^{\mathrm{rst}} = T_{2\mathrm{to}3}\, y_j^{\alpha\beta}, \qquad (8)$$

where $j \in \{a, b, c\}$ and $y \in \{u, i, i_o\}$, it follows

$$L_k \frac{d}{dt} i_k^{\alpha\beta} = -R_k i_k^{\alpha\beta} + u_k^{\alpha\beta}, \qquad (9a)$$

$$L_c \frac{d}{dt} i_c^{\alpha\beta} = -R_c i_c^{\alpha\beta} + u_a^{\alpha\beta} - u_b^{\alpha\beta}, \qquad (9b)$$

and

$$u_k^{\alpha\beta} = \begin{bmatrix} u_k^\alpha \\ u_k^\beta \end{bmatrix} = \sqrt{2} \begin{bmatrix} U_k\cos\theta_k \\ U_k\sin\theta_k \end{bmatrix}, \qquad (10a)$$

$$i_{ok}^{\alpha\beta} = \begin{bmatrix} i_{ok}^\alpha \\ i_{ok}^\beta \end{bmatrix} = \sqrt{2} \begin{bmatrix} I_{ok}\cos(\theta_k + \varphi_k) \\ I_{ok}\sin(\theta_k + \varphi_k) \end{bmatrix}, \qquad (10b)$$

$$i_k^{\alpha\beta} = \begin{bmatrix} i_k^\alpha \\ i_k^\beta \end{bmatrix} = \sqrt{2} \begin{bmatrix} I_k\cos(\theta_k + \phi_k) \\ I_k\sin(\theta_k + \phi_k) \end{bmatrix}, \qquad (10c)$$

$$i_c^{\alpha\beta} = \begin{bmatrix} i_c^\alpha \\ i_c^\beta \end{bmatrix} = \sqrt{2} \begin{bmatrix} I_c\cos(\theta_a + x_a) \\ I_c\sin(\theta_a + x_a) \end{bmatrix}. \qquad (10d)$$

For each k-th voltage and current expressed with respect to the corresponding k-th reference frame define, then, the k-th rotation matrix

$$\Gamma(\theta_j) = \begin{bmatrix} \cos\theta_j & -\sin\theta_j \\ \sin\theta_j & \cos\theta_j \end{bmatrix}, \qquad (11)$$

where $j \in \{a, b, c\}$. Let us apply (11) to each k-th voltage and current in (9) in order to deal with demodulated voltages and currents, that is define

$$y_j^{\alpha\beta} = \Gamma(\theta_j)\, y_j^{\mathrm{dq}}, \qquad (12)$$

with $y \in \{u, i, i_o\}$. Therefore, by substituting (12) in (9) it follows

$$L_k \frac{d}{dt} i_k^{\mathrm{dq}} = -R_k i_k^{\mathrm{dq}} - L_k \Omega \frac{d}{dt}\theta_k\, i_k^{\mathrm{dq}} + u_k^{\mathrm{dq}}, \qquad (13a)$$

$$L_c \frac{d}{dt} i_c^{\mathrm{dq}} = -R_c i_c^{\mathrm{dq}} - L_c \Omega \frac{d}{dt}\theta_a\, i_c^{\mathrm{dq}} + u_a^{\mathrm{dq}} - \Gamma(\delta)^{-1} u_b^{\mathrm{dq}}, \qquad (13b)$$

where $k = a, b$, $\delta = \theta_a - \theta_b$, and we used

$$\Gamma(\theta_k)^{-1} \frac{d}{dt}\Gamma(\theta_k) = \begin{bmatrix} 0 & -1 \\ 1 & 0 \end{bmatrix} \frac{d}{dt}\theta_k = \Omega\, \frac{d}{dt}\theta_k, \qquad (14)$$

and

$$u_k^{\mathrm{dq}} = \begin{bmatrix} u_k^d \\ u_k^q \end{bmatrix} = \begin{bmatrix} U_k \\ 0 \end{bmatrix}, \qquad (15a)$$

$$i_k^{\mathrm{dq}} = \begin{bmatrix} i_k^d \\ i_k^q \end{bmatrix} = \begin{bmatrix} I_k\cos\phi_k \\ I_k\sin\phi_k \end{bmatrix}, \qquad (15b)$$

$$i_c^{\mathrm{dq}} = \begin{bmatrix} i_c^d \\ i_c^q \end{bmatrix} = \begin{bmatrix} I_c\cos x_a \\ I_c\sin x_a \end{bmatrix}. \qquad (15c)$$

The k-th inverter output current i_{ok}^{rst} defined in (2) can be written in the rotating dq reference frame by substituting (2) in (12) with (8), getting

$$i_{ok}^{\mathrm{dq}} = \Gamma(\theta_k)\, T_{3\mathrm{to}2}\, i_{ok}^{\mathrm{rst}}, \qquad (16)$$
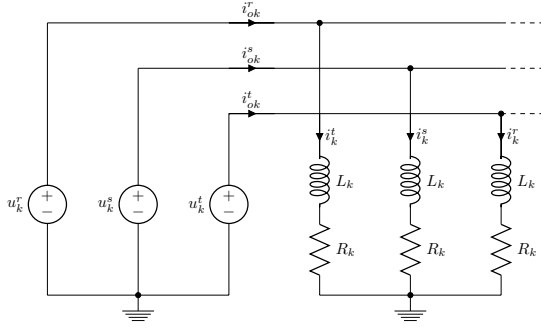
Fig. 2. Equivalent circuit of the k-th three-phase inverter and the corresponding local load.

where $k = a, b$. Let

$$\Gamma_k(\delta) = \begin{cases} I & k = a, \\ -\Gamma(\delta) & k = b, \end{cases} \tag{17}$$

where I is the identity matrix of suitable dimensions. Then the Kirckhhoff current laws allow to write

$$i_{ok}^{\mathrm{dq}} = i_k^{\mathrm{dq}} + \Gamma_k(\delta)^{-1} i_c^{\mathrm{dq}}, \tag{18}$$

with $k = a, b$. The dynamic model (13) together with the frequency and voltage droop controller equations will be used in next Sections for the closed loop stability analysis.

III. CLOSED LOOP MODEL

The closed loop model of (13) is obtained by determining the amplitude U_k and the frequency $(d/dt)\theta_k$ of each k-th voltage, with $k = a, b$, according to the frequency and voltage droop laws

$$\frac{d}{dt}\theta_k = \omega + m_k(\bar{P}_k - P_k), \tag{19a}$$

$$U_k = \bar{U}_k + n_k(\bar{Q}_k - Q_k), \tag{19b}$$

where ω is the reference frequency of each inverter, $\bar{U}_k$ is the k-th voltage reference, m_k and n_k are the k-th frequency and voltage droop coefficients, $\bar{P}_k$ and $\bar{Q}_k$ are the k-th active and reactive power references, P_k and Q_k are the k-th active and reactive powers provided by the k-th inverter downstream the k-th measuring filter and $k = a, b$. Each k-th P_k and Q_k is given by

$$\tau_k^P \frac{d}{dt}P_k = -P_k + p_k, \tag{20a}$$

$$\tau_k^Q \frac{d}{dt}Q_k = -Q_k + q_k, \tag{20b}$$

where τ_k^P and τ_k^Q are the time-constants of the k-th first order measuring filter and p_k and q_k are the k-th instantaneous active and reactive powers defined as

$$p_k = (u_k^{\mathrm{dq}})^\top i_{ok}^{\mathrm{dq}}, \tag{21a}$$

$$q_k = (u_k^{\mathrm{dq}})^\top \Omega\, i_{ok}^{\mathrm{dq}}, \tag{21b}$$

where $k = a, b$, Ω is defined in (14) and u_k^{dq} and i_{ok}^{dq} are the k-th dq voltage and output current given by (15). Then, by substituting (18) in (21) and then in (20), it follows that the k-th active power P_k and reactive power Q_k are given by

$$\tau_k^P \frac{d}{dt}P_k = -P_k + (u_k^{\mathrm{dq}})^\top (i_k^{\mathrm{dq}} + \Gamma_k(\delta)^{-1} i_c^{\mathrm{dq}}), \tag{22a}$$

$$\tau_k^Q \frac{d}{dt}Q_k = -Q_k + (u_k^{\mathrm{dq}})^\top \Omega (i_k^{\mathrm{dq}} + \Gamma_k(\delta)^{-1} i_c^{\mathrm{dq}}). \tag{22b}$$

Therefore, the closed loop model of the microgrid is obtained by substituting (19b) in (15a) and then in (13) and (22), (19a) in (13) and recalling that $\delta = \theta_a - \theta_b$:

$$\frac{L_k}{R_k}\frac{d}{dt}i_k^{\mathrm{dq}} = -\left(I + \omega\frac{L_k}{R_k}\Omega\right)i_k^{\mathrm{dq}} - \frac{L_k}{R_k}\Omega m_k(\bar{P}_k - P_k)\, i_k^{\mathrm{dq}}$$
$$+ \frac{1}{R_k}[\bar{U}_k + n_k(\bar{Q}_k - Q_k)]\begin{bmatrix}1\\0\end{bmatrix}, \tag{23a}$$

$$\frac{L_c}{R_c}\frac{d}{dt}i_c^{\mathrm{dq}} = -\left(I + \omega\frac{L_c}{R_c}\Omega\right)i_c^{\mathrm{dq}} - \frac{L_c}{R_c}\Omega m_a(\bar{P}_a - P_a)\, i_c^{\mathrm{dq}}$$
$$+ \frac{1}{R_c}\sum_{k=a,b}\Gamma_k(\delta)^{-1}[\bar{U}_k + n_k(\bar{Q}_k - Q_k)]\begin{bmatrix}1\\0\end{bmatrix}, \tag{23b}$$

$$\tau_k^P \frac{d}{dt}P_k = -P_k + \begin{bmatrix}1 & 0\end{bmatrix}(i_k^{\mathrm{dq}} + \Gamma_k(\delta)^{-1} i_c^{\mathrm{dq}})\cdot$$
$$[\bar{U}_k + n_k(\bar{Q}_k - Q_k)], \tag{23c}$$

$$\tau_k^Q \frac{d}{dt}Q_k = -Q_k + \begin{bmatrix}1 & 0\end{bmatrix}\Omega(i_k^{\mathrm{dq}} + \Gamma_k(\delta)^{-1} i_c^{\mathrm{dq}})\cdot$$
$$[\bar{U}_k + n_k(\bar{Q}_k - Q_k)], \tag{23d}$$

$$\frac{d}{dt}\delta = m_a(\bar{P}_a - P_a) - m_b(\bar{P}_b - P_b), \tag{23e}$$

where $k = a, b$, and $\Gamma_k(\delta)$ and Ω are defined in (17) and (14), respectively. Typical values of the loads inductances L_k and resistances R_k, where $k = a, b$, allow to assume

$$\frac{L_k}{R_k} \ll \frac{L_c}{R_c}, \tag{24a}$$

$$\frac{L_k}{R_k} \ll \tau_k^P, \tag{24b}$$

$$\frac{L_k}{R_k} \ll \tau_k^Q. \tag{24c}$$

Therefore, by applying the singular perturbation technique [12] to (23), from (23a) one obtains

$$0 = -\left(I + \omega\frac{L_k}{R_k}\Omega\right)z_k^{\mathrm{dq}} + \frac{1}{R_k}[\bar{U}_k + n_k(\bar{Q}_k - Q_{z,k})]\begin{bmatrix}1\\0\end{bmatrix}, \tag{25}$$

where $k = a, b$, 'z' and $Q_{z,k}$ indicate the currents and the reactive power of the reduced order system, respectively. Notice that the assumption of small ratios L_k/R_k does not imply that $\omega(L_k/R_k)$ is small too. The reduced order model is obtained by substituting the soultions of (25) into (23b)–

(23e):

$$\frac{L_c}{R_c}\frac{d}{dt}z_c^{\mathrm{dq}} = -\left(I + \omega\frac{L_c}{R_c}\Omega\right)z_c^{\mathrm{dq}} - \frac{L_c}{R_c}\Omega m_a(\bar{P}_a - P_{z,a})\,z_c^{\mathrm{dq}}$$
$$+ \frac{1}{R_c}\sum_{k=a,b}\Gamma_k(\delta)^{-1}[\bar{U}_k + n_k(\bar{Q}_k - Q_{z,k})]\begin{bmatrix}1\\0\end{bmatrix},$$

(26a)

$$\tau_k^P\frac{d}{dt}P_{z,k} = -P_{z,k} + \begin{bmatrix}1 & 0\end{bmatrix}(z_k^{\mathrm{dq}} + \Gamma_k(\delta_z)^{-1}\,z_c^{\mathrm{dq}})\cdot$$
$$[\bar{U}_k + n_k(\bar{Q}_k - Q_{z,k})],$$

(26b)

$$\tau_k^Q\frac{d}{dt}Q_{z,k} = -Q_{z,k} + \begin{bmatrix}1 & 0\end{bmatrix}\Omega\,(z_k^{\mathrm{dq}} + \Gamma_k(\delta_z)^{-1}\,z_c^{\mathrm{dq}})\cdot$$
$$[\bar{U}_k + n_k(\bar{Q}_k - Q_{z,k})],$$

(26c)

$$\frac{d}{dt}\delta_z = m_a(\bar{P}_a - P_{z,a}) - m_b(\bar{P}_b - P_{z,b}),$$

(26d)

where $k = a, b$ and where δ_z and $P_{z,k}$ are the angle and the active power of the reduced order model. In next Section it is shown that the 7-th order model (26) is able to capture the stability property of the 11-th order closed loop model (23).

IV. SIMULATION RESULTS

The simulations have been carried out by considering the following realistic values of the control, loads and line parameters [13] for the microgrid depicted in Fig. 1: $m_a = 5\cdot10^{-4}$ rad/sW, $n_a = 5\cdot10^{-4}$ V/VAr, $\tau_a^P = 0.17$ s, $\tau_a^Q = 0.17$ s, $\bar{P}_a = 806$ W, $\bar{Q}_a = 384$ VAr, $\bar{U}_a = 127$ V, $R_a = 13$ Ω, $L_a = 16$ mH, $m_b = 5\cdot10^{-4}$ rad/sW, $n_b = 5\cdot10^{-4}$ V/VAr, $\tau_b^P = 0.17$ s, $\tau_b^Q = 0.17$ s, $\bar{P}_b = 750$ W, $\bar{Q}_b = 375$ VAr, $\bar{U}_b = 130$ V, $R_b = 25$ Ω, $L_b = 35$ mH, $R_c = 0.5$ Ω, $L_c = 8$ mH, $\omega = 2\pi 60$ rad/s. An equilibrium point of the closed loop system (23) is given by $i_a^{d,\mathrm{eq}} = 8.1$ A, $i_a^{q,\mathrm{eq}} = -3.7$ A, $P_a^{\mathrm{eq}} = 806.3$ W, $Q_a^{\mathrm{eq}} = 384.8$ VAr, $i_b^{d,\mathrm{eq}} = 4.1$ A, $i_b^{q,\mathrm{eq}} = -2.1$ A, $P_b^{\mathrm{eq}} = 750.3$ W, $Q_b^{\mathrm{eq}} = 374.1$ VAr, $i_c^{d,\mathrm{eq}} = -1.7$ A, $i_c^{q,\mathrm{eq}} = 0.7$ A, $\delta^{\mathrm{eq}} = -0.0368$ rad. The eigenvalues of the system's Jacobian computed around such equilibrium point are

$$\lambda_{1,2} = -861.81 \pm \jmath376.98, \tag{27a}$$
$$\lambda_{3,4} = -724.98 \pm \jmath376.99, \tag{27b}$$
$$\lambda_{5,6} = -62.72 \pm \jmath376.93, \tag{27c}$$
$$\lambda_{7,8} = -2.98 \pm \jmath4.82, \tag{27d}$$
$$\lambda_9 = -6.28, \tag{27e}$$
$$\lambda_{10} = -6.02, \tag{27f}$$
$$\lambda_{11} = -5.99, \tag{27g}$$

which show that the system is locally stable for the particular choice of the line, control and load parameteres. Fig. 3 and Fig. 4 show the time domain evolution of the local loads direct and quadrature currents and the time domain evolution of the inverters and line direct and quadrature currents, respectively. Fig. 4 particularly shows the presence of fast and slow modes in the inverters and line currents dynamics. By comparing Fig. 3 and Fig. 4 one can notice how the loads currents

evolve on the same small temporal scale of the fast modes which affect the inverters and line currents. In Fig. 5 are reported the time evolutions of the active powers P_a, P_b, and reactive powers Q_a, Q_b, of each inverter. Fig. 6 shows the time domain evolution of $\delta = \theta_a - \theta_b$. The inverters
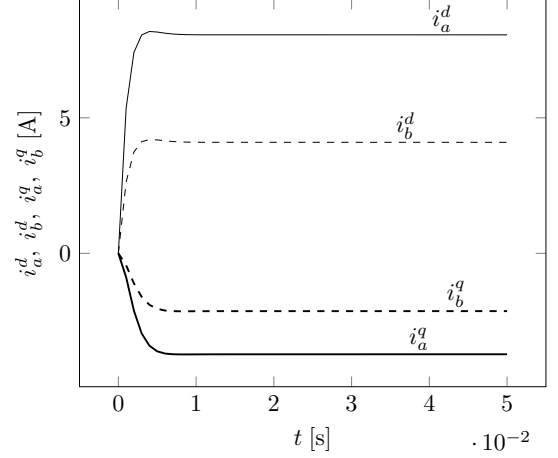
Fig. 3. Time domain evolution of the direct components i_a^d (solid line) and i_b^d (dashed line) of the load a and b currents and quadrature components i_a^q (solid thick line) and i_b^q (dashed thick line) of the load a and b currents for zero initial conditions, for $m_a = 5\cdot10^{-4}$.

start with the same angle, that is $\delta(0) = 0$, and in order to provide for the required active and reactive powers according to the corresponding reference values, at steady-state a non-zero angle difference is needed. Clearly, this depends also by the local loads. In Fig. 7 it is shown the time evolution of the instantaneous frequencies $(d/dt)\theta_a$ (solid line) and $(d/dt)\theta_b$ (dashed line) determined by the frequency droop laws. Each $(d/dt)\theta_k$ starts from the corresponding initial value given by $\omega + m_k\bar{P}_k$, where $k = a, b$. Then, both $(d/dt)\theta_a$ and $(d/dt)\theta_b$ converge to the same steady-state value given by the frequency reference $\omega = 2\pi 60$ rad/s since also P_a and P_b converge to $\bar{P}_a$ and $\bar{P}_b$, respectively. The stability of the closed loop system is influenced by the control parameters. Fig. 8 shows the eigenlocus for $m_a \in [5\cdot10^{-4}, 5\cdot10^{-1}]$. For each m_a the new equilibrium point, given by the solution of (23) obtained setting all the derivative terms to zero, has been computed and then used to determine the eigenvalues of the system's Jacobian. As it is shown, by increasing the frequency control parameter m_a some of the eigenvalues become positive real, and for $m_a \geq 1.8\cdot10^{-1}$ the system is unstable. Fig. 9 shows the eigenlocus for $\tau_a^P \in [0.017, 0.17]$ s. Particularly, the final value of the active power filter time-constant τ_a^P of the inverter a is $\tau_a^P = 0.17$ s, that is, the cut-off frequency of such active power filter is approximately an order of magnitude lower than the nominal frequency ω. The corresponding eigenlocus is drawn for $m_a = 5\cdot10^{-2}$ and for $\tau_a^P = 0.036$ s some eigenvalues become positive real. By comparing this result with those in [14], where it is shown that if no filters at all are used the system is unstable for $m_a = 2.4\cdot10^{-2}$, it is clear that by means of the active and reactive power filters the system local stability is improved for higher value of m_a. On the
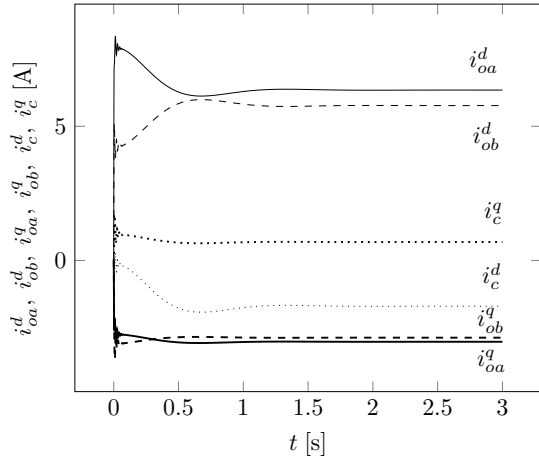
Fig. 4. Time domain evolution of the direct components i_{oa}^d (solid line), i_{ob}^d (dashed line), i_c^d (dotted line) and quadrature component i_{oa}^q (solid thick line), i_{ob}^q (dashed thick line), i_c^q (dotted thick line) of the inverters' and line direct and quadrature currents for zero initial conditions, for $m_a = 5 \cdot 10^{-4}$.
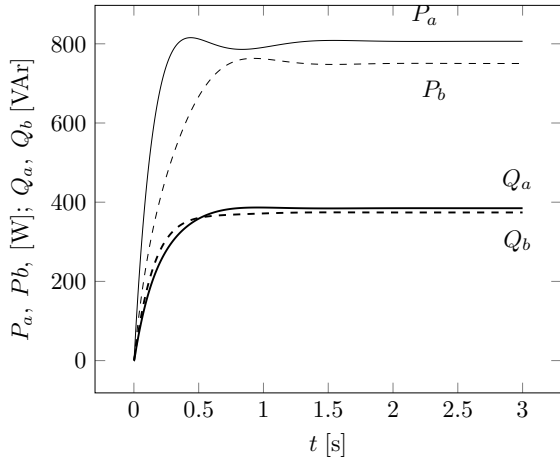

Fig. 6. Time domain evolution of the angle delay δ existing between the voltage u_a^{rst} and the voltage u_b^{rst} for zero initial conditions, for $m_a = 5 \cdot 10^{-4}$.

Fig. 5. Time domain evolution of the active powers P_a (solid line), P_b (dashed line) and reactive powers Q_a (solid thick line), Q_b (dashed thick line) provided by the inverters, for $m_a = 5 \cdot 10^{-4}$.

Fig. 7. Time domain evolution of the frequency $(d/dt)\theta_a$ (solid line) and $(d/dt)\theta_b$ (dashed line) of the voltage u_a and the voltage u_b provided by the microgrid inverters, for $m_a = 5 \cdot 10^{-4}$.

other hand, comparing the eigenvalues around the equilibrium point with those showed in [14], in case the filters are used the system response is slower for the same value of m_a. Fig. 8 and (27) show that, for $m_a = 5 \cdot 10^{-4}$, the linearized dynamic is approximately given by a seventh order system obtained by neglecting the fast eigenvalues $\lambda_{1,2}$ and $\lambda_{3,4}$. This is also justified by the singular perturbation approach used in Sec. III. As Fig. 10 shows, the eigenlocus of the linearized reduced order model system predicts the instabilities for the same value of m_a for which the full order system is unstable.
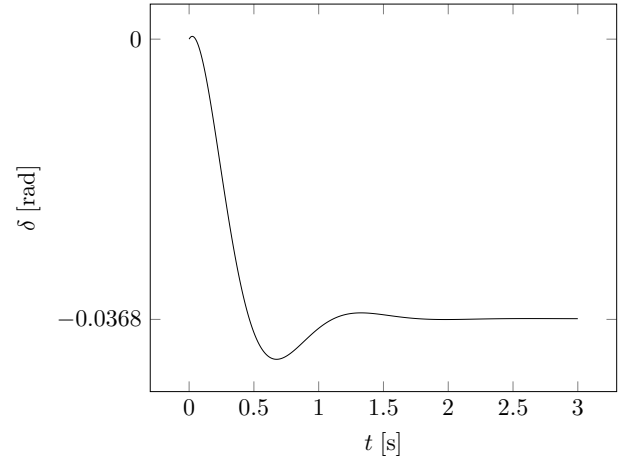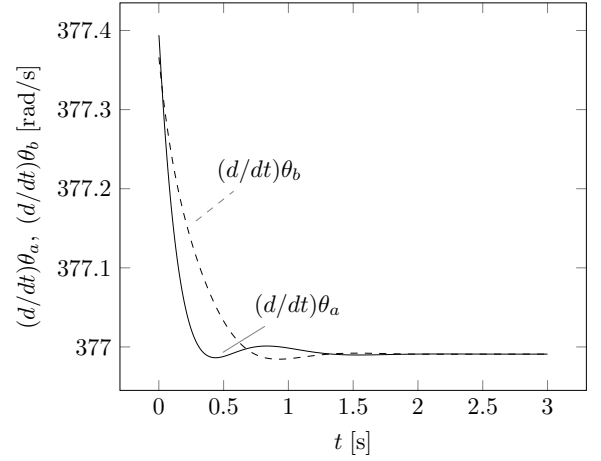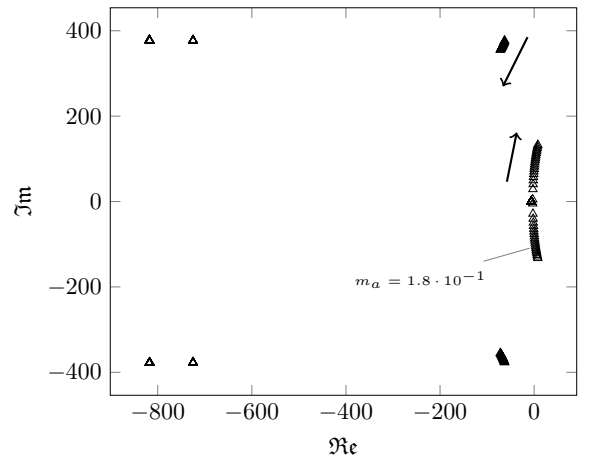

Fig. 8. Eigenlocus of the linearized system around the equilibrium point for $m_a \in [5 \cdot 10^{-4}, 5 \cdot 10^{-1}]$.
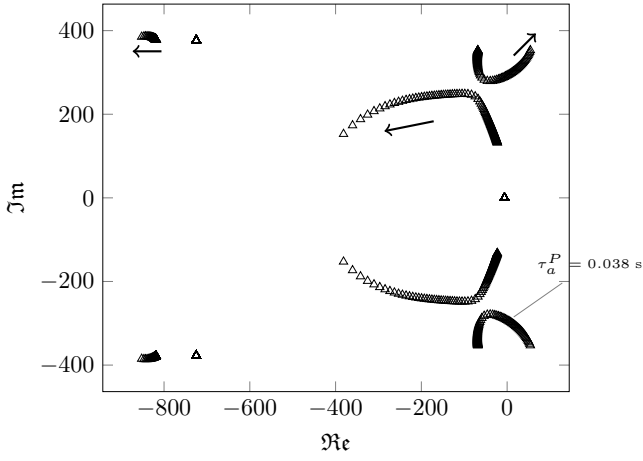
Fig. 9. Eigenlocus of the linearized system around the equilibrium point for $\tau_a^P \in [0.017, 0.17]$ s and $m_a = 5 \cdot 10^{-2}$.
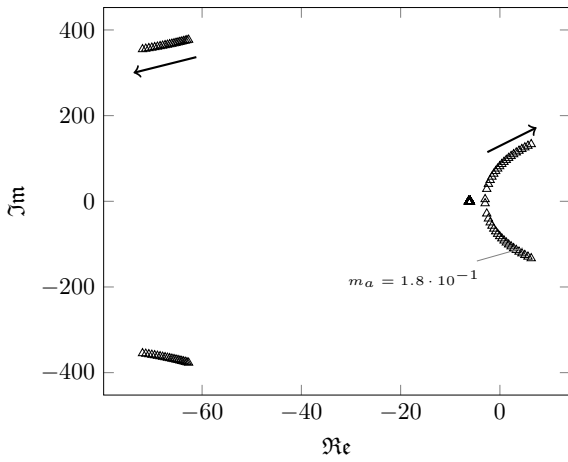

Fig. 10. Eigenlocus of the reduced order linearized system around the equilibrium point for $m_a \in [5 \cdot 10^{-4}, 5 \cdot 10^{-1}]$.

V. CONCLUSIONS

The proposed approach to model two droop controlled inverters forming a microgrid allows to compute the equilibrium points of the closed loop system and to carry out an eigenvalue analysis showing that for some values of the frequency droop control parameter m_a the system becomes unstable. The technique used allows also to assess that the nominal value of m_a the large signals dynamics are well approximated by those of a reduced order model derived by neglecting the loads dynamics, that is by applying a singular perturbation approach to the original model. Indeed, the reduced order model still allows to determine the value of m_a which makes the system unstable. The local stability properties of the system are improved by the presence of power filters also for quite large value of m_a, even though the dynamic response is slower than that of the same system without power filters. Similar considerations can be operated with different values of the remaining parameters.

REFERENCES

[1] J. M. Guerrero, M. Chandorkar, T.-L. Lee, and P. C. Loh, "Advanced Control Architectures for Intelligent Microgrids-Part I: Decentralized and Hierarchical Control," *IEEE Trans. on Industrial Electronics*, vol. 60, no. 4, pp. 1254–1262, 2013.
[2] Q.-C. Zhong, "Robust Droop Controller for Accurate Proportional Load Sharing Among Inverters Operated in Parallel," *IEEE Trans. on Industrial Electronics*, vol. 60, no. 4, pp. 1281–1290, 2013.
[3] Y. Mohamed and E. El-Saadany, "Adaptive Decentralized Droop Controller to Preserve Power Sharing Stability of Paralleled Inverters in Distributed Generation Microgrids," *IEEE Trans. on Power Electronics*, vol. 23, no. 6, pp. 2806–2816, 2008.
[4] N. Pogaku, M. Prodanovic, and T. C. Green, "Modeling, Analysis and Testing of Autonomous Operation of an Inverter-Based Microgrid," *IEEE Trans. on Power Electronics*, vol. 22, no. 2, pp. 613–625, 2007.
[5] I. Serban and C. Marinescu, "Enhanced Control Strategy of Three-Phase Battery Energy Storage Systems for Frequency Support in Microgrids and With Uninterrupted Supply of Local Loads," *IEEE Trans. on Power Electronics*, no. 99, p. 1, 2013.
[6] L. Wang, X. Q. Guo, H. R. Gu, W. Y. Wu, and J. M. Guerrero, "Precise Modeling Based on Dynamic Phasors for Droop-Controlled Parallel-Connected Inverters," in *Proc. of the 21st International Symposium on Industrial Electronics*, Hangzhou, China, 2012, pp. 475–480.
[7] S. Tabatabaee, H. R. Karshenas, A. Bakhshai, and P. Jain, "Investigation of Droop Characteristics and X/R Ratio on Small-Signal Stability of Autonomous Microgrid," in *Proc. of the 2nd Power Electronics, Drive Systems and Technologies Conference*, Tehran, Iran, February 2011, pp. 223–228.
[8] J. W. S.-Porco, F. Dorfler, and F. Bullo, "Synchronization and Power Sharing for Droop-Controlled Inverters in Islanded Microgrids," *Automatica*, vol. 49, no. 9, pp. 2603–2611, 2013.
[9] V. Mariani and F. Vasca, "Stability Analysis of Droop Controlled Inverters via Dynamic Phasors and Contraction Theory," in *Proc. of the 12th European Control Conference*, Zurich, Switzerland, July 2013, pp. 1505–1510.
[10] ——, "Partial Contraction Analysis for Droop Controlled Inverters," in *Proc. of the 3rd International Conference on Systems and Control*, Algiers, Algeria, October 2013.
[11] E. Clarke, *Circuit Analysis of AC Power Systems*. New York: Wiley, 1943, vol. 1.
[12] H. K. Khalil, *Nonlinear Systems*, 3rd ed. New Jersey: Prentice Hall, 2002.
[13] E. A. A. Coelho, P. C. Cortizo, and P. F. D. Garcia, "Small-Signal Stability for Parallel-Connected Inverters in Stand-Alone AC Supply Systems," *IEEE Trans. on Industry Applications*, vol. 38, no. 2, pp. 533–542, 2002.
[14] V. Mariani, F. Vasca, and J. M. Guerrero, "Dynamic-Phasor-Based Nonlinear Modelling of AC Islanded Microgrids Under Droop Control," in *Proc. of 11th International Multi-Conference on Systems, Signals and Devices*, Barcelona, Spain, February 2014.